Special Issue

http://dx.doi.org/10.3786/sincs2011.21

NANO-MICRO LETTERS ARTICLE

www.nmletters.org

(Proceedings of 2011 Shanghai International Nanotechnology Cooperation Symposium, SINCS 2011, Published online 10 January 2012)

# Nanocrystallization Kinetics of Amorphous $Fe_{84}Nb_7B_9$ Alloy

Wei LU[1,2*], Chenchong He[1,2], Zhe Chen[1,2], Biao YAN[1,2]

**Abstract:** The nanocrystallization kinetics of amorphous $Fe_{84}Nb_7B_9$ alloy has been analyzed by non-isothermal DSC measurements. The local activation energies E($\alpha$) were analyzed and its average value was about 468.7 kJ/mol. It was found that the nanocrystallization kinetics of amorphous $Fe_{84}Nb_7B_9$ alloy cannot be described successfully by JMA model while the two-parameter Sestak-Bergggren equation seems to be more appropriate in this case. However, SB model has only a phenomenological value and gives no insight on the interpretation of the nanocrystallization mechanisms of $Fe_{84}Nb_7B_9$ alloy. So the local activation energies and local Avrami exponent were introduced and they were applicable and correct in describing the nanocrystallization process of the amorphous $Fe_{84}Nb_7B_9$ alloy according to the theoretical DSC curve simulation.

**Keywords:** Amorphous $Fe_{84}Nb_7B_9$ alloy; Crystallization kinetics; Activation energy; JMA model

**Citation:** Wei LU, Chenchong He, Zhe Chen and Biao YAN, "Nanocrystallization Kinetics of Amorphous $Fe_{84}Nb_7B_9$ Alloy", Proceedings of Shanghai International Nanotechnology Cooperation Symposium, 84-89 (2011). http://dx.doi.org/10.3786/sincs2011.21

## Introduction

Soft magnetic alloys consisting of nanoscale bcc Fe grains have been developed by primary crystallization of melt-spun amorphous alloys, as typically exemplified in Fe–Si–B–Nb–Cu (Finemet) [1] and Fe-M-B (M=Zr, Hf, Nb) (Nanoperm) [2] systems. Among these nanocrystalline alloys, the Fe-M-B (M=Zr, Hf, Nb) alloys, such as $Fe_{90}Zr_7B_3$, $Fe_{84}Nb_7B_9$ and $Fe_{89}Hf_7B_4$, are particularly attractive because of the simplicity of the alloy system as well as their high saturation magnetization. Various research literatures reveal that the properties of nanocrystalline materials are closely related to their composition and the thermal treatment they experienced [3-6]. The related studies are still carried out widely. But in these studies, most of them are reported on nanocrystallization in Fe-Zr-B and Fe-Zr-B-Cu alloys, little is known about the crystallization behavior especially the crystallization kinetics in M=Nb or Hf alloys.

Generally, because of the very small sizes (~10nm) of the crystallites, the experimental data of the nanocrystallization kinetics of Fe-based amorphous alloys are always analyzed within the framework of nucleation and growth by the well-known JMA model based on a few of assumptions, which is applicable only to particularly simple cases meeting the needs of the site saturation condition [7]. Any of the quantitative evaluations of experimental thermal analysis (TA) data, the authors think, must be preceded first by checking if the JMA model is suitable for describing the alloy system to be researched. But it seems that the checking is not taken in all the studies where the crystallization kinetics of Fe-based amorphous alloys has been carried out.

Therefore, the aim of this paper is to give a detailed investigation on the nanocrystallization kinetics of $Fe_{84}Nb_7B_9$ alloy considering the validity of JMA model and give a detailed explanation on it according to the determination of variable local activation energy Ec($\alpha$) and local Avrami exponent n($\alpha$) during the

School of Materials Science and Engineering[1], Shanghai Key Lab. of D&A for Metal-Functional Materials[2], Tongji University, Shanghai 200092, China
*Corresponding author. E-mail:

nanocrystallization by differential scanning calorimetry (DSC) at various heating rates. In addition, the theoretical DSC curve taking account of the variable kinetic parameters was calculated, which is well fitted with the experimental DSC curve.

## Experiment

The amorphous ribbons of $Fe_{84}Nb_7B_9$ alloy were prepared by a single-roller melt spinning technique on a copper wheel in Ar atmosphere and the sample dimensions are 10 mm wide and 20 mm thick. The nanocrystallization kinetics of amorphous $Fe_{84}Nb_7B_9$ alloy was investigated with a NETZSCH-STA449C TG/DSC instrument using a continuous heating regime with heating rates $\beta$ from 5 to 30℃/min. A $N_2$ gas flow was used for the ambient atmosphere. The temperature axis as well as the enthalpy axis was calibrated using indium and zinc standards for all the heating rates. X-ray diffraction confirms the amorphous nature of the as-quenched ribbons.

## Results and discussion

The non-isothermal nanocrystallization process of amorphous $Fe_{84}Nb_7B_9$ alloy at different heating rates exhibits a single exothermal peak in the DSC curves which are normalized with sample weight, as shown in Fig. 1. It is evident that this exothermal peak corresponds to the nanocrystallization of $\alpha$-Fe grains as identified by XRD diffraction analysis.

For the study of crystallization kinetics we assume that each crystallization peak can be described by a kinetic equation of the form

$$\frac{d\alpha}{dt} = k\,(T)\,f\,(\alpha)\,, \tag{1}$$

where

$$k\,(T) = A\exp\,(-E/RT)\,, \tag{2}$$

is the Arrhenius temperature-dependent rate constant, $E$ is the activation energy, $A$ is the pre-exponential factor and $f(\alpha)$ characterizes the type of transformation mechanism.

The activation energy E is one of the most important kinetic parameters for the crystallization of an amorphous alloy. Generally, the nanocrystallization of amorphous $Fe_{84}Nb_7B_9$ alloy is accompanied by nucleation and growth of crystal phases under continuously varied conditions of chemical surroundings in the zone of conversion. For instance, solute B atoms are rejected into the glassy matrix during the transformation. Thus the free enthalpy difference between the crystalline and the amorphous phases also changes, so that the corresponding driving force for crystallization is dependent on the fraction already transformed. Also, the kinetic parameters (i.e. crystallization condition), such as diffusion coefficient, are composition-dependent, and will change as the crystallization proceeds. Such changes of crystallization condition can result in a change of the activation energy and even the mechanism of the crystallization process. It is, therefore, necessary to study the change in activation energy and mechanism of an amorphous alloy during crystallization. So, a local activation energy $E(\alpha)$, which presents the activation energy at a stage when the crystallized volume fraction is $\alpha$, was applied to describe the variable activation energy which reflects the change of nucleation and growth behavior in the crystallization process in present paper. In this paper, an isoconversional method without assuming the kinetic model function is used to determined the value of $E(\alpha)$ [8,9]. This model-free method is expressed as

$$\left[\frac{d\ln\phi}{d\,(1/T)}\right]_{\alpha} = -\frac{E}{R} \tag{3}$$

where, R is gas constant, T and $\phi$ are the temperatures and specific heat flow (w/g) corresponding to fixed values of $\alpha$ from experiments at different heating rates $\beta$, respectively.

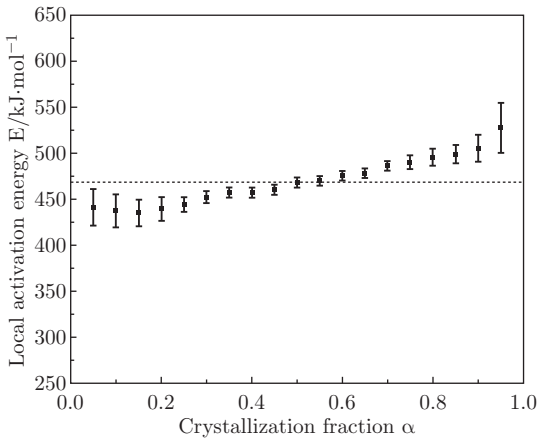


By using the experimental data of $\phi$-$T$ at different heating rates, we plot $ln\phi$ vs. $1/T$ with a certain value of $\alpha$, and $E_c(\alpha)$ is obtained from the slope of the straight line for a constant $\alpha$. Figure 2 shows the relationship between crystallized volume fraction and local activation energy of amorphous $Fe_{84}Nb_7B_9$ alloy. It is seen that at the initial crystallization stage, the local activation energies for crystallization of amorphous $Fe_{84}Nb_7B_9$ alloy lies in the range of 435 kJ/mol∼440 kJ/mol ($0<\alpha<0.2$). When the crystallized volume fraction falls in the range of 0.2∼0.9, the local activation energy of the amorphous $Fe_{84}Nb_7B_9$ alloy increases from 440 kJ/mol to about 500kJ/mol slowly. At the last stage of primary crystallization ($\alpha>0.9$), the local activation energy increases sharply and is up to 527

kJ/mol when $\alpha$ is about 0.95. The average activation energy for the whole nanocrystallization of amorphous $Fe_{84}Nb_7B_9$ alloy is about 468.7 kJ/mol, which is just between the activation energy values obtained from the Kissinger equation (460.8±16 kJ/mol) and Ozawa equation (473.6±16 kJ/mol) in present experiments and has a good agreement with them.

The E values obtained above for amorphous $Fe_{84}Nb_7B_9$ alloy are higher than Finemet (around 380 kJ/mol). In amorphous $Fe_{84}Nb_7B_9$ alloy, Nb atom is an obstacle for the growth of nanocrystallized grains, so the activation energy of crystal growth is considerably large. Provided that the activation energy of crystal growth ($E_g$) is higher than that of nucleation ($E_n$), the high E value can be attributed to a significant contribution of crystal growth to the whole nanocrystallization process. Another possible reasons for the unusually high activation energy in this study is the deviation of experimental results from an ideal Arrhenius type temperature dependence. It has previously been pointed out by Koster and Meinhardt [10] that the nucleation kinetics is governed by viscous flow as well as atomic diffusion in a temperature range around the glass transition temperature ($T_g$) and the nucleation frequency is accelerated significantly above $T_g$ by the contribution of viscous flow to the atomic transport.

The crystallization kinetics is usually interpreted in terms of the standard nucleation-growth model formulated by Johnson-Mehl-Avrami (JMA) [11]. The JMA equation can be described as

$$d\alpha/dt = kn\,(1-\alpha)\,\{\ln[1/(1-\alpha)]\}^{(n-1)/n}, \qquad (4)$$

where t is time, the rate constant $k$ is a function of temperature and in general depends on both the nucleation frequency and the crystal growth rate, and the kinetic exponent $n$ is a parameter which reflects the nucleation frequency and/or the growth morphology. Henderson [12,13] has shown that the validity of the JMA equation can be extended in non-isothermal conditions if the entire nucleation process takes place during the early stages of the transformation, and it becomes negligible afterward. The crystallization rate is controlled only by temperature and does not depend on the previous thermal history. Although the limits of applicability of the JMA equation are well known [12,13], in practice it is not so easy to verify whether the conditions of applicability are fulfilled or not. But Malek [14,15] has proposed a simpler method to test the applicability of the JMA model. The test is based on Eqs. (5) and (6) and on the y($\alpha$) and z($\alpha$) functions. Under non-isothermal conditions these functions are given by

$$y(\alpha) = \phi \exp\left(\frac{-E_a}{RT}\right) \qquad (5)$$

$$z(\alpha) = \phi T^2 \qquad (6)$$

where $\phi$(w/g) is the heat flow. For practical reasons the y($\alpha$) and z($\alpha$) functions are normalized within the (0,1) range. If there is a maximum of the y($\alpha$) function at $\alpha_m \in$(0,1), the kinetic data can be described by the JMA (n>1). The functions of z($\alpha$) also has a maximum at $\alpha_p^\infty$. This parameter has a characteristic value $\alpha_p^\infty \cong 0.632$ for the JMA model.

Figure 3 shows y($\alpha$) and z($\alpha$) varying with crystalline fraction $\alpha$. It is evident that the traces by y($\alpha$) and z($\alpha$) were nearly independent of heating rate. The value of $\alpha_m$ and $\alpha_p^\infty$ in functions y($\alpha$) and z($\alpha$) are shown in Table 1. The value of $\alpha_m$ show that the kinetic data can be described by JMA(n>1) model. But the $\alpha_p^\infty$ is far lower than the value predicted for JMA model (0.61∼0.65), it seems that one or more conditions for the applicability of the JMA model is not fulfilled in the nanocrystallization kinetics of $Fe_{84}Nb_7B_9$ alloy. Another test of the applicability of JMA model is the linearity of the double logarithmic plots vs. lnt or 1/T. Such plots obtained from non-isothermal DSC data for the nanocrystallization of $Fe_{84}Nb_7B_9$ alloy are shown in Fig. 4. The plots are clearly non-linear, indicating that the JMA model cannot be applied. The above two results are consistent with each other.

As mentioned above, the JMA model can not be used to describe the crystallization kinetics of $Fe_{84}Nb_7B_9$ alloy. During the formation of the primary nanocrystals, the rejection of the insoluble atoms will cause the formation of a concentration gradient ahead of the nucleating front. Such concentration gradients have already been deduced from the experimentally determined evolution of the magnetic properties of the residual amorphous phase during crystallization of Nb-containing Fe-based amorphous alloys [16-18] and measured ahead of primary nucleating fronts in AlCeNi-type amorphous alloys [19]. This situation indicates that the site saturation condition is no longer held. As a consequence, the maximum of the z($\alpha$) function is differ from its theoretical value for JMA model. In this case, it is convenient to use more flexible empirical kinetic model functions, f($\alpha$), for the description of crystallization process, e.g. the Sestak-Berggren (SB) empirical kinetic model:

$$f(\alpha) = \alpha^m (1-\alpha)^n, \qquad (7)$$

where the parameters m and n define the relative contributions of acceleratory and decay regions of the kinetic process and they are also taken as kinetic parameters describing the shape of measured TA curve. The SB model is applicable in the crystallization kinetics of $Fe_{84}Nb_7B_9$ alloy according to the value of $\alpha_m$ and $\alpha_p^\infty$ in functions y($\alpha$) and z($\alpha$) and the diagram proposed by Malek [20].

For SB (m,n) model, the kinetic parameter ratio, p=m/n, is calculated using the following formula,

$$p = \alpha_m/(1-\alpha_m) \qquad (8)$$

and n can be obtained by the following formula,

$$\ln\left[(d\alpha/dt)\, e^{x}\right] = \ln A + n \ln\left[\alpha^{p}\,(1-\alpha)\right]. \qquad (9)$$

That is, the kinetic parameter n corresponds to the slope of the linear plot of $\ln[(\mathrm{d}\alpha/\mathrm{dt})\mathrm{e}^{x}]$ vs. $\ln[\alpha^{p}(1-\alpha)]$ for $\alpha \in (0.2, 0.8)$. Then the second kinetic exponent is m=pn.

Using formula (8) and (9), the kinetic parameters in SB(m, n) model of nanocrystallization for Finemet alloy are calculated and shown in Table 2. The average value of n was 2.31 and m was 0.18. The high value of n>1 means a complex kinetic process involving both nucleation and growth. These results can be applied to explain the variable E described in above.

**Table 1 The value of $\alpha_m$ and $\alpha_p^{\infty}$ in functions y($\alpha$) and z($\alpha$) at different heating rates.**

| Heating rate $\beta$ (℃/min) | $\alpha_m$ | $\alpha_p^{\infty}$ |
|---|---|---|
| 5 | 0.0727 | 0.4333 |
| 10 | 0.0827 | 0.4159 |
| 17.5 | 0.0689 | 0.4165 |
| 30 | 0.0654 | 0.4508 |

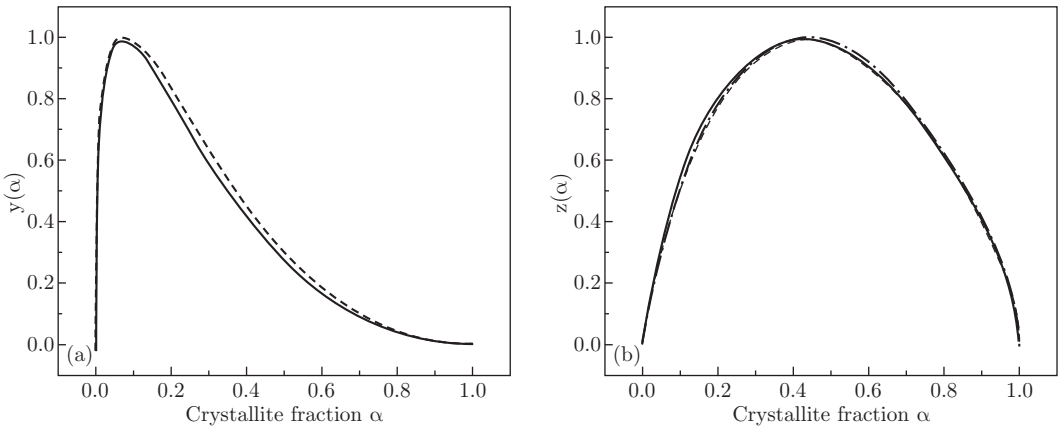


Fig. 3 Normalized y($\alpha$) (A) and z($\alpha$) (B) functions obtained by transformation of non-isothermal DSC data for $Fe_{84}Nb_7B_9$ alloy. The heating rates are shown by lines: 5℃/min (solid line); 10℃/min (dash line); 17.5℃/min (dot line); 30℃/min (dash dot line).

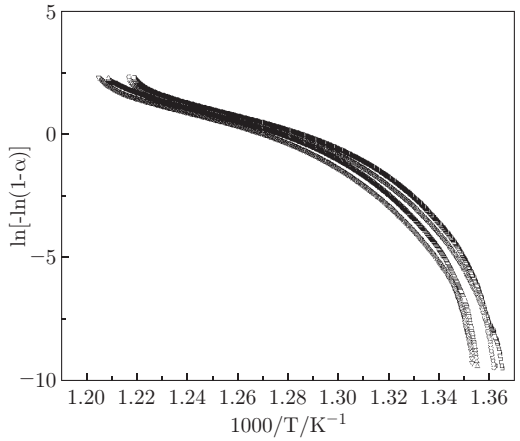


Fig. 4 The double logarithmic plots obtained from DSC data shown in Fig. 1 as a function of 1/T.

**Table 2 Kinetic parameters of SB (m, n) model calculated from DSC data using equations (8) and (9).**

| Heating rate $\beta$ (℃/min) | p | n | m |
|---|---|---|---|
| 5 | 0.0784 | 2.33 | 0.18 |
| 12.5 | 0.0902 | 2.33 | 0.21 |
| 17.5 | 0.0740 | 2.32 | 0.17 |
| 30 | 0.0699 | 2.26 | 0.16 |

However, SB model has only a phenomenological value and gives no insight on the interpretation of the nanocrystallization mechanisms of $Fe_{84}Nb_7B_9$ alloy. In order to give a detailed explanation on it, we introduce a local Avrami exponent, n($\alpha$) [21], to describe the detailed mechanism of the nanocrystallization of amorphous $Fe_{84}Nb_7B_9$ alloy. But this equation is only applicable for isothermal crystallization. In Ref.[22], we deduced a new equation in order to calculate the local Avrami exponent for non-isothermal crystallization and it is expressed as follow:

$$n(\alpha) = \frac{-R\partial \ln\left[-\ln(1-\alpha)\right]}{E(\alpha)\partial\,(1/T)} \qquad (10)$$

Taking account of the variable local activation energy E($\alpha$), the local Avrami exponents n($\alpha$) at heating rate of 5 ℃/min were calculated. Figure 5 shows the value of local Avrami exponent of amorphous $Fe_{84}Nb_7B_9$ alloy during primary crystallization. It can be seen that the value of n($\alpha$) varies significantly with $\alpha$ over the whole primary crystallization process. Initially, n($\alpha$) is about 4.0. With the progress of crystallization, n($\alpha$) decreases slowly from 4.0 to about 0.8 when $\alpha$ reaches 0.95. However, when the crystallized fraction is higher than 0.95, the local Avrami exponent increases rapidly

to 1.4. The n($\alpha$)-$\alpha$ dependence curves obtained at other heating rates are similar to this one.

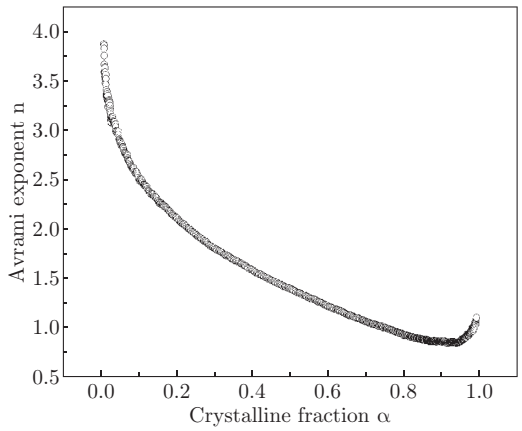


Fig. 5 Local Avrami exponent n($\alpha$) as a function of crystallized fraction $\alpha$ at heating rate of 5 ℃/min.

At the beginning of the primary crystallization ($\alpha$ <0.02), the calculated local Avrami exponent n is about 4.0. But because of the large uncertainties caused in calculating $n$ based on the DSC data which rely on the choice of baseline in region $\alpha$ <0.02, the value of $n$ for $\alpha$ <0.02 is not taken into consideration. So, in the initial stage (0< $\alpha$ <0.2), the local Avrami exponent n($\alpha$) is in the range of 2.0∼4.0, which means that two and three dimensional nucleation and grain growth controlled by diffusion at decreasing nucleation rate are dominant for bulk crystallization in this stage. In the middle stage (0.2< $\alpha$ <0.95), the n($\alpha$) decreases from about 2.0 to about 0.8 with the increasing crystallized fraction. This result indicates that one dimensional nucleation and grain growth at a near-zero nucleation rate are responsible for surface crystallization. From the variation of n($\alpha$), this kind of growth mode is dominant during non-isothermal primary crystallization process. In the final stage ($\alpha$ > 0.95), the local Avrami exponents n($\alpha$) rise sharply to about 1.4. The anomalous rise of local Avrami exponents n($\alpha$) at high $\alpha$ has also been observed in the primary crystallization processes of various metallic glasses [23∼26]. As discussed in reference [26], if there exist inhomogeneously distributed pre-existing nuclei in the amorphous ribbons, and/or a inhomogeneous nucleation occurs in the crystallization process, anomalous Avrami exponent will be expected, especially at high $\alpha$, just as what have been observed in references [23∼25]. So the inhomogeneous distribution of nuclei in the amorphous samples may be one important factor resulting in the widely observed anomalous Avrami exponent. In present paper, the anomalous Avrami exponent n($\alpha$) at high $\alpha$ is mainly because of the exhaustion of pre-existing nuclei of $\alpha$-Fe grains and the formation of some $\alpha$-Fe grains quickly growing up to almost the final sizes.

In order to test the correctness of local activation energies and local Avrami exponents, the JMA theoretical DSC curves with and without assuming non-linear relationships between kinetic parameters (local activation energy Ec($\alpha$) and local Avrami exponent n($\alpha$)) and crystallization fraction $\alpha$ shown in Figs. 2 and 5 were calculated. The theoretical and experimental DSC curves are all shown in Fig. 6 for comparison. It is evident that the theoretical DSC curve taking accounting of variable local activation energy Ec($\alpha$) and local Avrami exponent n($\alpha$) fits the experimental DSC curve well while the theoretical curve based on only constant activation energy and Avrami exponent does not. So, one may expect that the variable local activation energies Ec($\alpha$) and local Avrami exponents n($\alpha$) are applicable and correct in describing the primary crystallization process of the amorphous Finemet alloy while the constant activation energy and Avrami exponent are not.

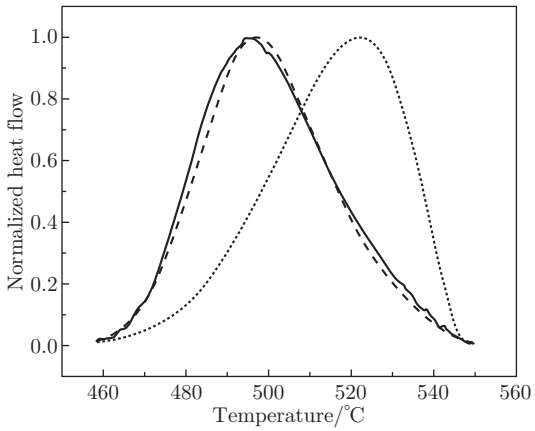


Fig. 6 Theoretical and experimental DSC curves at heating rate of 5 ℃/min. Experimental curve (solid line); JMA theoretical curve using constant activation energy and Avrami exponent (dotted line); JMA theoretical curve using variable activation energies and Avrami exponents (dash line).

## Conclusions

The nanocrystallization kinetics of amorphous $Fe_{84}Nb_7B_9$ alloy was investigated by DSC using various heating rates in present paper. The local activation energy E($\alpha$) was determined by an isoconversional method without assuming the kinetic model function. It was found that the local activation energy E($\alpha$) changed with crystalline fraction $\alpha$ and the average value was about 468.7 kJ/mol. The nanocrystallization kinetics of amorphous $Fe_{84}Nb_7B_9$ alloy cannot be described successfully by JMA model and the two-parameter Sestak-Bergggren equation seems to be more appropriate in this case. However, SB model has only a phenomenological value and gives no insight on the interpretation of the nanocrystallization mechanisms of $Fe_{84}Nb_7B_9$ alloy. The local activation

energies and local Avrami exponent were introduced to describe the nanocrystallization mechanisms. The significant variation of local Avrami exponent and local activation energy with crystallized volume fraction demonstrates that the nanocrystallization kinetics of amorphous $Fe_{84}Nb_7B_9$ alloy varies at different stages and the variable local activation energies $Ec(\alpha)$ and local Avrami exponents $n(\alpha)$ are applicable and correct in describing the primary crystallization process of the amorphous $Fe_{84}Nb_7B_9$ alloy according to the theoretical DSC curve simulation.

## Acknowledgements

The partial financial support of the Shanghai Science and Technology Committee (Grant No. 0352nm057 and 04DZ05616) is gratefully acknowledged.

## References

[1] Y. Yoshizawa, S. Oguma and K. Yamauchi, J. Appl. Phys. 64, 6044 (1988).

[2] K. Suzuki, A. Makino, A. Inoue and T. Matsumoto, J. Appl. Phys. 74, 3316 (1993).

[3] H. Lee, K. J. Lee, Y. K. Kim, K. Kim and S. C. Yu, J. All. Comps. 326, 313 (2001).

[4] J. D. Ayers, V. G. Harris, J. A. Sprague, W. T. Elam and H. N. Jones , Acta. Mater. 46, 1861 (1998).

[5] J. Moya, M. Vazquez, V. Cremaschi, B. Arcondo and H. Sirkin , Nanostruct. Mater. 8, 611 (1997).

[6] J. Gonzalez, N. Murillo, J. M. Blanco, J. M. Gonzalez and T. Kulik, J. Appl. Phys. 76, 1131 (1994).

[7] J.W. Christian, The Theory of Transformations in Metals and Alloys, 2nd ed., Pergamon Press, New York, (1975).

[8] H. L. Friedman, J. Polym. Sci. Part C: Polym. Lett. 6, 183 (1964).

[9] T. Ozawa, J. Therm. Anal. 31: 547 (1986).

[10] U. Koster and J. Meinhardt, Mater. Sci. Eng. A178, 271 (1994).

[11] W. Lu, Y. Lei, B. Yan and W. Huang, phys. stat. sol. (a) 202, 1733 (2005).

[12] D. W. Henderson, J. Thermal Anal. 15, 325 (1979).

[13] D. W. Henderson, J. Non-Cryst. Solids 30, 301 (1979).

[14] J. Malek, Thermochimica Acta 267, 61 (1995).

[15] J. Malek, Thermochimica Acta 138, 337 (1989).

[16] A. R. Yavari and D. Negri, NanoStruct. Mater. 8, 969 (1997).

[17] T. Kulik and A. Hernando, J. Magn. Mag. Mater. 138, 270 (1994).

[18] S. D. Kaloshkin, I. A. Tomilin, B. V. Jalnin, I. B. Kekalo and E. V. Shelekhov, Mater. Sci. Forum 179, 557 (1995).

[19] K. Hono, Y. Zhang, A. P. Tsai, A. Inoue and Sakurai T, Scripta Metall. Mater. 32, 191 (1995).

[20] J. Malek and V. Smrcka, Thermochimica Acta 186, 153 (1991).

[21] A. Calka and A. P. Radlinski, J. Mater. Res. 3, 59 (1985).

[22] W. Lu, B. Yan and W. Huang, J. Non-Cryst, Solids 351, 3320 (2005).

[23] G. Ghosh, M. Chandrasekaran and L. Delaey, Acta Metall. Mater. 39, 925 (1991).

[24] N. X. Sun, K. Zhang, X. H. Zhang, X. D. Liu and K. Lu, Nanostruct. Mater. 7, 637 (1996).

[25] K. Lu, X. D. Liu and F. H. Yuan , Physica B. 217,, 153 (1996).

[26] N. X. Sun, X. D. Liu and K. Lu, Scripta Materialia 34, 1201 (1996).